Pseudomorphic-to-bulk fcc phase transition of thin Ni films on Pd(100)

G. A. Rizzi,[1] A. Cossaro,[2] M. Petukhov,[1,*] F. Sedona,[1] G. Granozzi,[1] F. Bruno,[2] D. Cvetko,[2,†] A. Morgante,[2,‡] and L. Floreano[2,§]

[1]*Dipartimento di Scienze Chimiche and INFM Research Unit, University of Padova, Via Loredan 4, I-35131 Padova, Italy*

[2]*Laboratorio TASC dell'Istituto Nazionale per la Fisica della Materia, Basovizza SS-14, Km 163.5, I-34012 Trieste, Italy*

(Received 13 January 2004; revised manuscript received 9 April 2004; published 16 July 2004)

We have measured the transformation of pseudomorphic Ni films on Pd(100) into their bulk fcc phase as a function of the film thickness. We made use of x-ray diffraction and x-ray induced photoemission to study the evolution of the Ni film and its interface with the substrate. The growth of a film with tetragonally strained face centered symmetry (fct) has been observed by out-of-plane x-ray diffraction up to a limit thickness of 10 Ni pseudomorphic layers (some of them partially filled and intermixed with the substrate), where a new fcc bulklike phase is formed. After the formation of the bulklike Ni domains, we observed the pseudomorphic fct domains to disappear preserving the number of layers and their spacing. The phase transition thus proceeds via lateral growth of the bulklike phase within the pseudomorphic one, i.e., the bulklike fcc domains penetrate down to the substrate when formed. This large depth of the walls separating the domains of different phases is also indicated by the increase of the intermixing at the substrate–film interface, which starts at the onset of the transition and continues at even larger thickness. The bulklike fcc phase is also slightly strained; its relaxation towards the orthomorphic lattice structure proceeds slowly with the film thickness, being not yet completed at the maximum thickness presently studied of 30 Å (~17 layers).

DOI: 10.1103/PhysRevB.70.045412 PACS number(s): 68.55.Jk, 61.10.Nz, 79.60.−i, 68.35.Rh

I. INTRODUCTION

Heterogeneous epitaxy is a widely exploited technique to fabricate artificial materials since it allows one to introduce a controlled degree of distortion of the interatomic bond length and orientation, which finally allows one to tune the electronic properties of nanostructured devices. In the case of semiconductors, the strain of a film growing on a heterogeneous substrate can be retained up to a thickness of several hundreds of nanometers (coherent growth). Beyond this critical thickness, the strain is released through the formation of a pattern of misfit dislocations, which propagate from the interface to the surface and drive the gradual relaxation (decoherence) of the growing film to its bulk structure. Thanks to the high degree of long range order, the mechanism for semiconductor decoherence can be followed and described in much detail.[1] While a reduced misfit is required for coherent semiconductor growth, thin artificial phases with a lattice structure much different from the bulk one can be stabilized for metal film growth. In the case of oxide substrates, the decoherence of metal films through and ordered network of misfit dislocations is usually observed when the misfit does not exceed ~10%.[2] On the other hand, the metal bonding allows the strain to be released on a much smaller thickness scale, thus reducing the average domain size of the growing film, i.e., the probability of detecting any long range order behavior. Things are getting more complicated when metal on metal heteroepitaxy is considered, since intermixing phenomena have also to be taken into account, which can either favor the stabilization of pseudomorphic films via surfactant effect [like for the Fe/Au(100) system[3,4]] or inhibit the coherent growth via substrate roughening and alloying [like for the Co/Cu(111) system[5]].

In the past 10 years, metal heteroepitaxy has been widely applied to study magnetic systems, since the magnetic behavior of metals (both spin orientation and magnetic moment)[6] and their chemical reactivity can be modified by appropriate distortion of their lattice structure. These metastable artificial phases are decomposed into their ground structural phase when the films exceed a critical thickness of a few layers. These transformations are usually observed to be rather sharp and occur through a rather abrupt nondiffusive distortion mechanism, which is accompanied by a strong morphological reorganization, like for the much studied Fe/Cu(100) system,[7,8] thus smearing the mechanisms of domain growth.

In fact, most of the studies have been performed by means of low-energy electron diffraction (LEED), ion scattering, and scanning tunnel microscopy (STM), i.e., surface sensitive techniques. The behavior of the interface and of the layers beneath the surface is poorly known and is usually obtained by photoelectron diffraction (XPD) experiments at a Synchrotron facility, where the photoelectron kinetic energy can be effectively tuned to change the penetration depth. On the other hand, XPD data require a rather complex analysis, whose reliability is hampered when the number of scatterers (penetration depth) is increased.[9] Grazing incidence x-ray diffraction (GIXRD) is certainly the best suited technique to study the structure of a buried interface and the layered structure of thin films.[2] Recently, a combination of XPD and GIXRD techniques has been applied to study the structural dependence on thickness of Fe films on $Cu_3Au(100)$ from a pseudomorphic phase to the bcc one.[10] The structural transformation has been shown to be characterized by phase coexistence over a thickness range of a few monolayers.

Hereafter, we have applied GIXRD to study the structure of thin Ni films grown on Pd(100). The epitaxial growth of ultrathin Ni films on the Pd(100) surface has been recently

studied by means of LEED, XPS, and XPD with a laboratory x-ray source.[11] This study has shown that in the early stages of the deposition there is the formation of a tetragonally strained face centered (fct) Ni phase with the same lateral lattice spacing of the substrate (i.e., 3.89 Å) and a vertical compression of 0.24 Å. When the film thickness exceeds a critical value of approximately 9–12 layers, the film transforms into its bulklike Ni fcc structure (lattice parameter of 3.52 Å). The measured strain of the fct phase is found to be in full agreement with the elasticity theory, but some open questions still remain. In particular, although capable to measure very nicely the tetragonal strain adopted by the Ni film, the XPD data did not yield any clear information on how the phase transition develops as the critical thickness is approached nor was it straightforward to extract information on the film/substrate interface. For all these reasons we decided to perform a more detailed study on this system taking advantage of the unique possibilities to acquire *in situ* XPS, XPD, and GIXRD data offered by the ALOISA beamline at ELETTRA Synchrotron (Trieste, Italy).

An effective limit thickness for the pseudomorphic growth has been found. The transformation into the Ni bulklike structure is shown to involve the interface as well, where the intermixing increases. In addition, the number of layers in the residual pseudomorphic fct phase does not change during the transformation, but simply its domains shrink. The transformation thus proceeds via lateral growth of the bulklike Ni phase. The increase of the intermixing beyond the critical thickness is attributed to the lateral propagation of the defects, which drive the transformation of the pseudomorphic phase.

II. EXPERIMENT

Both electron spectroscopy and x-ray surface diffraction measurements have been performed *in situ* at the ALOISA beamline, where a wide photon energy range (130–8000 eV), coupled to a multiple detection system, is available.[12] The UHV experimental chamber (base pressure in the 10^{-11} mBar range) hosts hemispherical electron analyzers and x-ray detectors. The emission direction from the sample surface can be freely selected for any orientation of the surface. The sample is mounted on a 6-degrees-of-freedom manipulator, specially designed to select with great accuracy (0.01°) the orientation of the surface with respect to the incoming photon beam. The temperature of the sample, measured by thermocouples, can be varied by resistive heating and liquid nitrogen cooling.

The Pd(100) substrate was prepared by Ar^+ sputtering at 1 keV and annealing to 970 K. The substrate order was checked by reflection high-energy electron diffraction, while XPS surveys at grazing incidence (of the order of the critical angle) were used to check for residual contamination. Nickel was evaporated from a carefully outgassed electron bombardment cell (Omicron) provided with a water cooled shield. The sample was kept at room temperature for all the Ni depositions, but the thinnest one (2.5 Å), grown at 330 K. A quartz microbalance allowed us to tune the deposition flux at a constant rate of ~0.6 Å/min (10% accuracy) before deposition. The absolute calibration of the growth rate was determined *a posteriori* by measuring the x-ray reflectivity (XRR) at fixed scattering angle while scanning the photon energy between 3 and 8 keV. The interference between the x-ray scattering from the substrate–film and film–vacuum interfaces gives rise to maxima and minima as a function of the perpendicular momentum transfer. Fitting to the XRR curves with a simple model of regularly spaced bulk layers thus yields the film effective thickness (from the position of maxima and minima) and the width of the interfaces (from the amplitude of the oscillation), as shown in Fig. 1. Hereafter the films of different thickness will be labeled by a nominal coverage (in Angstrom), corresponding to their Ni bulk equivalent thickness.

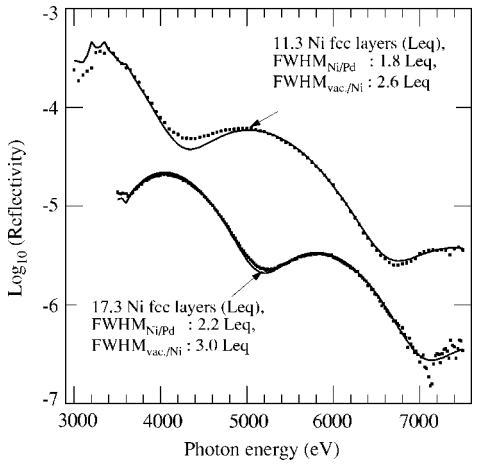

FIG. 1. Logarithm of the x-ray reflectivity energy scan (dots), taken at fixed scattering angles of 7° and 6° for two films of ~22 and ~30 Å, respectively. The two curves have been shifted for the sake of clarity. The film thickness and interface widths are expressed as Ni fcc layer-equivalent (Leq) after fitting to the experimental data (full lines) with a simple Ni/Pd bulk model. The Ni/Pd and vacuum/Ni interfaces are assumed to have a Gaussian depth profile, whose widths full width at half maximum are also indicated in the figure legend.

For each Ni film, we measured both in-plane XRD and XPS from the Pd 3*d* core level and the valence band (VB), while XPD polar scans from the Ni $2p_{3/2}$ were surveyed for a better comparison with previous experiments. The in-plane XRD measurements consist of radial scans across the $(\bar{2}0\ 0)$ peak in the Pd(100) reciprocal lattice. These measurements were taken scanning the photon energy in a broad range under a suitable θ–2θ scattering geometry. The observation of diffraction peaks in radial scans allows us to determine the lateral lattice spacing d through the Bragg condition $2d \sin\theta = hc/E$. Out-of-plane XRD (rod scans) has been taken for a few selected films in the critical thickness range to determine the perpendicular distribution of the Ni layer spacings in the pseudomorphic phase. The $(\bar{2}\ 0\ L)$ rods of the Pd(100) substrate were taken at a photon energy of 7000 eV with a sampling of $\Delta L = 0.03$, up to $L = 2.2$. For each L value, we performed an azimuthal scan of the sample, while keeping widely open the detector slit in the direction parallel to the footprint of the x-ray beam, in order to collect

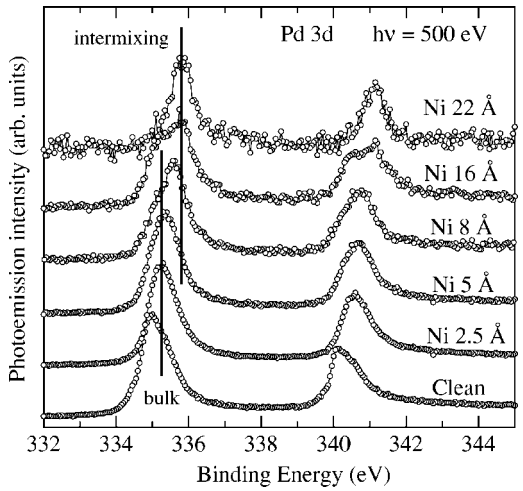

FIG. 2. Pd 3*d* photoemission spectra taken at a photon energy of 500 eV with an overall energy resolution of ~210 meV. The spectra are not to scale and they have been amplified and vertically shifted for a better comparison of the shape changes. The bulk component is the shoulder at 335.2 eV binding energy of the Pd 3*d* spectrum taken on the clean Pd substrate (bottom curve). The surface component yields a core level shift of −0.35 eV to lower binding energy. As Ni is deposited, a new component, due to Pd–Ni alloying, appears at a binding energy higher than the bulk one. The Pd surface component fully disappears after the deposition of 5 Å of Ni. The interface component is the main component at 16 Å and beyond. The vertical bars mark the binding energies of the bulk and interface components. Each spectrum is labeled by its nominal coverage.

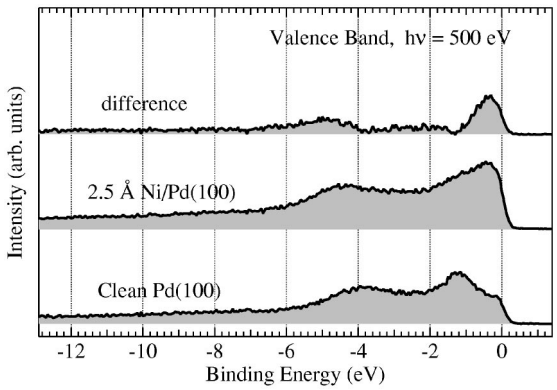

FIG. 3. Valence band of the Pd(100) sample before and after deposition of 2.5 Å of Ni. The curves have been vertically shifted for the sake of clarity. The top curve represents the difference spectrum of the former ones and puts in evidence the satellite peak at −5 eV, which is due to Pd–Ni alloying.

the whole diffracted intensity. Rod scan simulations were performed by the Vlieg's program ROD.[13]

Both Pd 3*d* and valence band photoemission spectra were taken at a photon energy of 500 eV with a photon energy resolution of ~125 meV. The surface was kept at a grazing angle of 4°, in transverse magnetic (i.e., *p*) polarization and the electron spectrometer was placed along the surface normal with a kinetic energy resolution of 170 meV. XPD polar scans of the Ni $2p_{3/2}$ peak (at $h\nu$=1270 eV) were measured in the same scattering conditions by rotating the electron analyzer in the scattering plane. We considered emission along the two main symmetry directions ⟨100⟩ and ⟨110⟩ of the substrate unit cell. We followed the procedure of Ref. 14 to extract the anisotropy component from the XPD polar scans by subtracting an isotropic component, which accounts for both geometrical (field of view, illuminated area) and physical (photoemission matrix symmetry, escape depth, surface roughness) factors.

III. RESULTS

A. Photoemission

The Pd 3*d* XPS data (with an overall energy resolution of about 200 meV) are reported in Fig. 2. We have analyzed the XPS spectra by fitting to Voigt functions and using a Shirley background. The Pd $3d_{5/2}$ peak of the clean substrate can be fitted with two components, one corresponding to the bulk peak (335.2 eV) and the other to the surface (334.85 eV), in agreement with previously reported data.[15] Upon Ni deposition the surface component is replaced by a new one at 335.85 eV, which is shifted by 0.65 eV from the bulk component, towards higher binding energies, as can be clearly seen in Fig. 2, where both components are well resolved in the 16 Å Ni coverage film. The bulk component disappears after the deposition of 22 Å of Ni. From comparison with valence band photoemission and photoelectron diffraction in the early stage of deposition, we have attributed the new Pd 3*d* component to the Pd–Ni alloying at the interface.

In fact, the formation of an intermixed phase at the beginning of the deposition is witnessed by the VB photoemission data of Fig. 3, taken just after the deposition of 2.5 Å of Ni. The upper part of the figure shows the difference spectra obtained by subtracting the clean Pd VB spectrum, multiplied by the proper attenuation factor, from the 2.5 Å Ni/Pd(100) spectrum. The result represents the film VB, where the peak at a binding energy of 5 eV cannot be found in the VB of neither pure Ni(100) nor Pd(100). It is worth reminding that the so-called "6 eV satellite" of the Ni 2*p* spectrum is found shifted to lower binding energies in the 2.5 Å film with respect to the same satellite for a thick film of 22 bulk monolayers.[11] Both the VB behavior and the shift to higher binding energy of the Pd $3d_{5/2}$ core level are the fingerprint of the intermixing process at the Ni/Pd interface, i.e., to the formation of a NiPd alloy in agreement with literature data.[16]

The intensity variation of the Pd $3d_{5/2}$ peak with the coverage of the Ni film is reported in Fig. 4 (upper panel). The bulk and interface components do not follow the same trend. The bulk component can be nicely fitted to a simple exponential decay, where the mean free path has been fixed to 4.6 Å, as calculated with the TPP-2 algorithm,[17] and the only free parameter is the Ni film growth rate. As can be seen from the upper panel of Fig. 4, the interface component requires a more complex function. It is important to note that the growth rate, as determined from the fitting procedure of the Pd 3*d* bulk component (0.6±0.1 Å/min), is in good agreement with the one obtained from the reflectivity curves

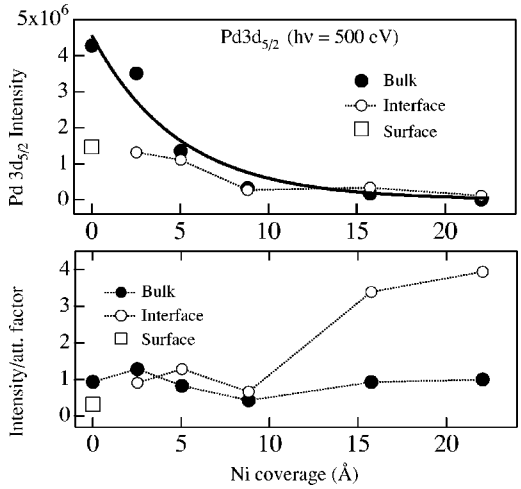

FIG. 4. Upper panel: intensity of the components of the Pd $3d_{5/2}$ photoemission peak (markers) as a function of the coverage of the Ni films (see text for the calibration of the film coverage). The full line is a fit to the bulk component (closed circles) with an exponential decay. The interface component (dotted line and open circles) follows a different decay law. Lower panel: intensity of the bulk (closed circles) and interface (open circles) Pd $3d_{5/2}$ components, after normalization to the attenuation factor yielded by the exponential decay of the Pd bulk component.

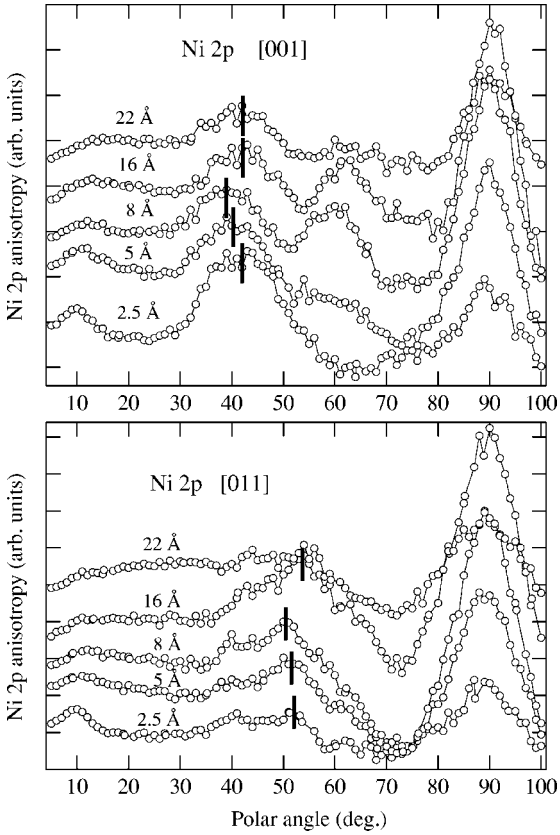

FIG. 5. Anisotropy of the polar scans taken for the Ni $2p_{3/2}$ photoelectron peak (kinetic energy of ~415 eV) along the ⟨100⟩ and ⟨011⟩ substrate symmetry directions, upper and lower panel, respectively. The curves have been vertically shifted for a better comparison. The vertical bars indicate the angular position of the forward scattering focusing peaks which are characteristic of an fcc symmetry. Deviations from the nominal values, i.e., 45° and 54.7° from the surface, are mainly due to distortions of the lattice cell in the topmost layers (which changes with the film coverage).

$(0.62 \pm 0.04$ Å/min), measured on the thicker films shown in Fig. 1. The fact that the Pd 3*d* signal completely disappears by further deposition (e.g., for a 30 Å Ni film) and that the Pd interface component only increases beyond a coverage of 8 Å, where the film is fully wetting the substrate (as demonstrated by the next XRD analysis), implies that no Pd surface segregation occurs in the present experimental conditions (room temperature growth). The increasing weight of the interface component is well represented in Fig. 4 (lower panel), where the ratio between the experimental values and the attenuation law, obtained from the bulk component, is reported. According to the figure, the interface component is the dominating one at 16 Å and beyond.

From the structural point of view, the intermixing at the interface determines an enhanced pseudomorphism at the early stages of Ni deposition. This can be observed from the coverage dependence of the forward scattering peaks originated by focusing from close-compact atom row directions in Ni $2p_{3/2}$ XPD polar scans, as shown in Fig. 5. At 2.5 Å, the fcc characteristic peaks are closer to the nominal fcc position (at 45° and 54.7° from the surface plane) than at higher coverage. The prominent forward scattering peak along the surface normal, indicative of a third layer formation, is due to both intermixing and cluster growth in the early stage of deposition. By increasing the film thickness, the forward scattering peaks shift away from the surface normal, indicating an increase of the vertical compression due to the elastic strain. The strain is released at 16 Å by the transformation into the bulklike Ni structure, in full agreement with previous XPD studies.[11]

B. X-ray diffraction

The Ni film transformation from the pseudomorphic fct phase to the bulk-like one does not occur through a continuous relaxation of the strained lattice cell, rather domains of bulk-like symmetry are formed at 16 Å, which grow in size as the coverage is increased. This transformation is clearly seen in Fig. 6, where in-plane radial scans across the substrate $(\bar{2}\ 0\ 0)$ XRD peak are shown for a few films of different coverage. Besides the substrate peak, a new feature appears at a coverage of 16 Å, corresponding to a lattice spacing of ~3.65 Å. This feature evolves shortly into a well-defined peak (see scan at 22 Å) which gradually shifts towards the 3.52 Å lattice parameter of fcc Ni. The appearance of the Ni bulklike peak at ~3.65 Å is the fingerprint of a structural phase transition.

For a better understanding of the structural transformation, we have studied the layer spacing distribution in the pseudomorphic fct Ni film. The XRD $(2\ 0\ L)$ rod scans are shown in Fig. 7 for a few films in the range of the critical thickness of 12–16 Å. The XRD scan along the substrate peak rod puts in evidence the x-ray scattering interference between the Ni pseudomorphic layers which are confined between the film–substrate and film–vacuum interfaces. If the deposition is homogeneous on the substrate, well-defined

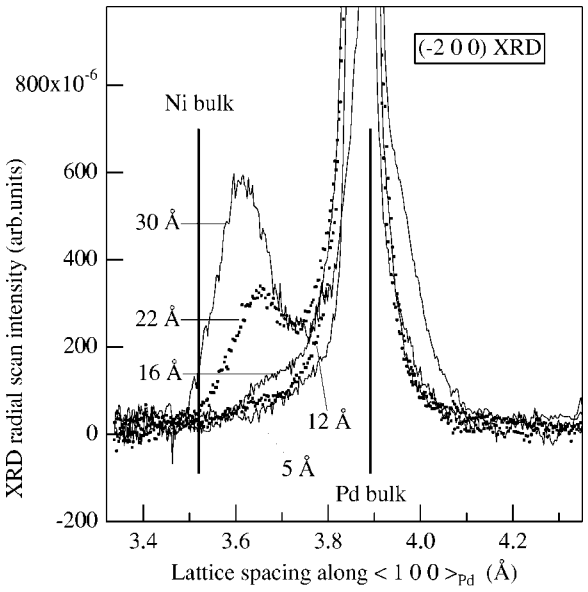

FIG. 6. Radial scans of the $(\bar{2}\ 0\ 0)$ XRD peak for a few Ni films of different coverage (alternating full and dotted lines). The XRD measurements have been taken by scanning the photon energy between 5400 and 7000 eV at fixed scattering geometry. The photon beam impinges the surface at grazing incidence, forming an angle $\theta \sim 35°$ with respect to the fcc(100) planes of the direct lattice. The substrate XRD peak is always out of scale, and the corresponding lattice spacing is indicated by the thick vertical line, as well as the lattice spacing of bulk fcc Ni.

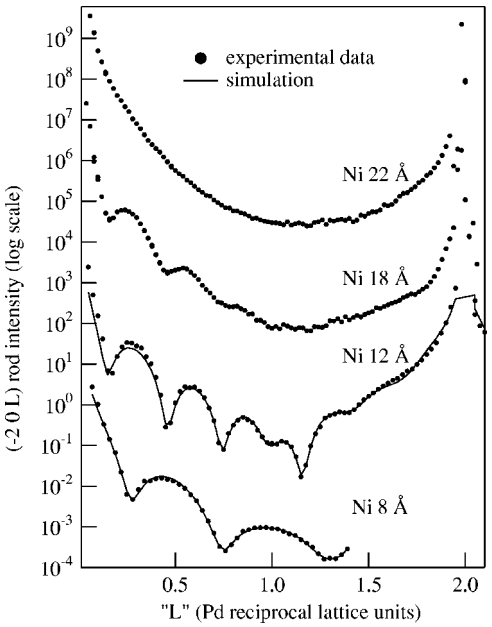

FIG. 7. Integrated intensity of the XRD $(\bar{2}\ 0\ L)$ rods of Pd for a few Ni films of different coverage (closed markers). The curves have been vertically shifted for the sake of clarity. Modulations in the low coverage films arise from Bragg interference among the Ni pseudomorphic layers, which are confined between sharp interfaces at both the top and bottom of the film. Fitting to the data (full lines) yields a structural model as reported in Table I.

interference oscillations can be seen along the rod scans, as in the case of the 8 and 12 Å films. The number of maxima and minima and their position is related to the number of Ni layers in the pseudomorphic structure, while the amplitude of the oscillations to the sharpness of the Ni film interfaces (the larger the amplitude the sharper the interface). The increased number of maxima and minima from the 8 Å film to the 12 Å one is thus reflecting the increased number of Ni layers in the pseudomorphic structure. The rod scan taken at 18 Å, where the Ni film structural transition has already started, is still showing a few faint modulations indicating that residual domains of the pseudomorphic phase are still coexisting with the fcc Ni phase. Most strikingly, the maxima and minima of the 18 Å phase still occur at the same perpendicular momentum transfer of the 12 Å film, i.e., the residual domains of the pseudomorphic phase contain the same number of Ni layers. The strong damping of the maxima and minima amplitude indicates both an increase of the pseudomorphic fct phase roughness and the deprival of the pseudomorphic Ni layers due to the shrinking of the corresponding domains. At the coverage of 22 Å, the whole film has been transformed into the Ni bulklike phase and the rod scan displays a structureless smooth behavior, which is characteristic of a bulk-truncated crystal surface.

The layer spacings and fillings for the 8 and 12 Å films have been obtained by fitting the rod scans with the structural model reported in Table I. Due to the large number of fitting parameters, we have fixed the inner layer spacings to the value determined by PED analysis after Ref. 11, and we focused our attention to the substrate–film and film–vacuum interfaces, where XRD yields the best sensitivity. With these constraints, we have found that the topmost layer is also compressed, in excellent agreement with previous XPD studies,[11] while the layers close to the film–substrate interface are expanded, confirming the vertical pseudomorphism indicated by the present XPD scan on very thin Ni films (Fig. 5). Concerning the buried interface, we admitted Ni/Pd intermixing for two layers. While this model yields an excellent fitting for the thinnest film, a larger number of layers might be affected by the intermixing in the 12 Å film, as indicated by the incomplete layer filling of a few buried Ni layers (3rd to 5th) with respect to the intermediate ones. Alternatively, this finding could be the fingerprint of the formation of extended morphological defects at the Ni–Pd interface when the critical thickness is achieved.

IV. DISCUSSION

The evolution of the Ni/Pd(100) film, as a function of the Ni coverage, is described by the following sequence. In the early deposition stage a couple of intermixed layers are formed with strict pseudomorphic structure. Further deposition leads to the formation of strained layers whose lattice cell is pseudomorphic to the lateral substrate lattice, but presents a perpendicular compression in agreement with the elastic force constant model. This elastically strained structure builds up to a coverage of 12 Å, corresponding to a limit thickness of 10 layers (including at least two intermixed layers at the substrate-film interface), not all of them are equally occupied. Beyond this coverage, domains of bulklike struc-

TABLE I. Structural parameters used to fit the 8 and 12 Å rod scans. The indetermination on the layer spacing and fillings is ±0.05 Å and ±0.1, respectively. The indexing of the layers is relative to the topmost bulk Pd layer (0th Pd layer) for both Ni and Pd. Each Pd layer spacing is always referred to the underneath Pd layer. Each Ni layer spacing, but the 1st one, is always referred to the underneath Ni layer. See text for the explanation of the layer filling behavior.

	8 Å film			12 Å film	
Layer	Spacing	Filling	Layer	Spacing	Filling
			10th Ni	1.53	0.3
			9th Ni	1.52[a]	0.7
			8th Ni	1.52[a]	0.9
			7th Ni	1.52[a]	0.9
6th Ni	1.56	0.3	6th Ni	1.52[a]	1.0
5th Ni	1.52[a]	0.7	5th Ni	1.52[a]	0.9
4th Ni	1.52[a]	0.7	4th Ni	1.52[a]	0.8
3rd Ni	1.86	1.0	3rd Ni	1.82	0.7
2nd Ni[b]	1.83	0.8	2nd Ni[b]	1.82	0.7
2nd Pd[b]	2.07	0.2	2nd Pd[b]	2.05	0.2
1st Ni[b]	2.18	0.3	1st Ni[b]	2.08	0.3
1st Pd[b]	1.94	0.7	1st Pd[b]	1.90	0.7

[a]Fixed parameter, after Ref. 11.
[b]Intermixed layers.

ture are formed and the whole film structure is gradually changed through a first order phase transition. Phase coexistence is clearly observed up to 18 Å. The strain release at the phase transition is not complete and the bulklike phase gradually relaxes to the orthomorphic fcc phase with increasing thickness.

The formation of a few deposit layers with a full pseudomorphic structure (as indicated by the XPD scan in Fig. 5 and the rod scan analysis in Table I) was also observed for very thin films (2 to 3 monolayers) of Fe on $Cu_3Au(100)$[10,18] and Ni on Cu(100).[19] The highly strained structure of these layers is probably stabilized by the intermixing and might be a general behavior of metal heteroepitaxy, whenever alloying or surface segregation is chemically favored. In the present system, and before the phase transition, the degree of intermixing remains constant, i.e., the concentration of substrate atoms is much smaller in the next deposited layers. From the 3rd layer on, a compressed vertical spacing is established, in agreement with the value predicted by the elastic theory for the given in-plane expansion, dictated by the substrate lattice.

The sequence of rod scans in Fig. 7 clearly shows that there exists a maximum number of Ni layers that can be stabilized into a pseudomorphic structure (10 layers, including the intermixed ones), thus defining an effective critical thickness for the structural phase transition. This configuration is established at a coverage of 12 Å, corresponding to an effective thickness of ~7 bulk equivalent layers. Beyond this critical coverage, the roughness of the Ni surface measured by XRR is seen to remain about 20% of the film thickness (see Fig. 1), thus excluding a dewetting transition, i.e., a transition of the growth regime from two-dimensional (2D) to three-dimensional (3D). This finding is also consistent with the perfect exponential decay of the bulk Pd 3*d* signal as a function of the Ni film coverage (see upper panel of Fig. 4), witnessing a continuation of the 2D growth.

The fact that the maximum number of layers with pseudomorphic fct structure does not change throughout the transition, but simply the fct domains decrease their homogeneity and size, indicates that the transition takes place through the lateral growth of the Ni bulklike domains at the expense of the pseudomorphic fct phase. Thus the Ni bulklike domains are not floating on top of the pseudomorphic fct phase nor the transition simply proceeds layer by layer from top to the bottom, rather, when formed, the Ni bulklike domains involve locally all the film layers, down to the Ni/Pd interface. A possible model for the Ni bulklike domains could be that of wedges, with the apex at the substrate–film interface, which expand at the expense of the pseudomorphic phase. Since the phase transition involves three-dimensional domains, it must be of the first order type. No time evolution of the diffracted peaks has been observed at room temperature on the time scale of the experiments (a few hours for the rod scans), which indicates that the transition is kinetically slowed down by the film defects.

From the XPS analysis in Fig. 4, the intermixing at the Ni/Pd interface is observed to increase beyond the critical coverage. It is very tempting to associate the increase of the intermixing with the propagation of a defect from the Ni/Pd interface (whose early formation might be witnessed by the incomplete layer filling of the buried Ni layers at the critical coverage of 12 Å), which drives the transformation of the pseudomorphic fct phase. The Ni/Pd lattice mismatch of ~10%, although not so small, might still allow the formation of an ordered pattern of misfit dislocations originated by the stacking faults at the interface, which would yield characteristic satellites of the Bragg's peaks in the radial scans.[2] While we have not checked by in-plane XRD for these feature on nonequivalent diffraction peaks other than the $(\bar{2}\,0\,0)$ one,

LEED pictures taken at the critical thickness were reported to display a Moiré pattern with (10×10) periodicity.[11] These patterns clearly show one order of extra spots decorating the integer peaks along the $\langle011\rangle$ substrate symmetry directions, i.e., the direction of close-compact atom rows on the fcc(100) surface. From comparison with the present data (in particular with the intermixing behavior), we can say that the strain release indicated by the extra spots is not limited to the Ni film surface, rather the Moiré pattern is originated by defects extending down to the substrate.

The Ni/Pd(100) system, where the Ni film undergoes a structural transition between two phases with the same face centered (100) surface symmetry, resembles the behavior of the Fe/Cu(100) system, where a more dramatic structural change, from an fcc(100) to a bcc(110) phase, takes place. In the latter case, the transition of the Fe film was described through the formation of shear planes (from the film surface down to the substrate) along close-compact atom rows, which separate domains of different structural phase, like for a martensitic phase transition.[7] An alternative microscopic mechanism was proposed for the Fe fcc to bcc transition by the group Biedermann *et al.*[20] They observed the formation of small bulklike domains (needles) on the topmost Fe layers in the early deposition stages, which were claimed to drive the transition when the film thickness exceeds the critical one. This microscopic mechanism, for being compatible with our experimental evidences on the Ni/Pd(100) system, would require the needles to be dispersed on the film surface with a random crystallographic orientation [which is not the case for Fe/Cu(100), according to Ref. 20], otherwise they would be detected by in-plane XRD radial scans. Moreover, the needles should vertically extend down to the substrate to explain the observed behavior of the Ni−Pd interface, but the available STM observations confine them to the topmost layers.[20] In fact, a very recent STM study has demonstrated the martensitic Fe/Cu(100) transition to take place also in the absence of bulklike needles.[21]

Concerning the growth of the newly formed bulklike Ni domains, a mechanism like that driving the decoherence in semiconductor heteroepitaxy can be envisaged. The domain walls, either shear planes or misfit dislocations, propagate laterally on the Pd substrate, leaving behind a strongly intermixed region. This picture is fully consistent with the increase of the Ni/Pd intermixing, which is observed to continue beyond the critical thickness (as indicated both by XPS analysis and by the Ni/Pd interface width obtained by the XRR analysis, Fig. 1).

Finally the newly formed bulklike Ni film is still strained at small thickness (see radial scan at 22 Å in Fig. 6) and the relaxation to its bulk fcc structure proceeds gradually with increasing thickness. This gradual relaxation, witnessed by the radial scans of the in-plane lattice parameters, is also seen in the perpendicular layered structure of the film. In fact the simple bulk structural models used to simulate the XRR energy scans yields a fitting quality which clearly improves from the 22 to 30 Å film (see Fig. 1). Such a behavior is not surprising since it has been observed for other metal films. As an example, the bulk structure of Fe deposited on $Cu_3Au(100)$ (where the 7% lattice mismatch is even smaller than the present one) is not fully recovered even for film thickness of the order of hundreds of monolayers.[22,23]

V. CONCLUSIONS

We studied the growth of Ni on Pd(100) by XPS (both core levels and VB), XPD, XRR, and XRD (both in- and out-of-plane) techniques. In particular, we followed the structural evolution of the Ni films as a function of the thickness. After the formation of a couple of intermixed layers (which preserve a perpendicular spacing close to the substrate one) a laterally pseudomorphic phase, with a perpendicular strain in agreement with the elastic theory, takes place. This pseudomorphic fct structure is stable up to a limit thickness of 10 pseudomorphic layers (some of them are partially filled and/or intermixed at the interface), corresponding to a nominal coverage of 12 Å, i.e., ~7 Ni bulk layers. Further Ni deposition leads to a gradual structural transformation of the whole film into a Ni bulklike fcc phase. This phase transition, accompanied by an increase of intermixing at the Ni/Pd interface, proceeds through the lateral growth of the Ni bulklike domains at the expense of the pseudomorphic fct phase. The latter domains preserve their layered structure (maximum number of layers and corresponding spacings), while shrinking. Residual strain is still observed in the Ni bulklike phase at a thickness of 30 Å.

*Also at IGNP, Russian Research Center, Kurchatov Institute, Moscow, Russia.

†Permanent address: Department of Physics, University of Ljubljana, Ljubljana, Slovenia.

‡Also at Department of Physics, University of Trieste, Trieste, Italy.

§Corresponding author: FAX: +39-040-226767; Email address: floreano@tasc.infm.it

[1] For an overview of the thermodynamics of semiconductor heteroepitaxy see: Chap. 5 in *Materials Fundamentals of Molecular Beam Epitaxy*, edited by J. Y. Tsao (Academic Press, San Diego, CA, 1993).

[2] For an overview of semicoherent metal/oxide growth see: G. Renaud, Surf. Sci. Rep. **32**, 1 (1998).

[3] R. Opitz, S. Löbus, A. Thissen, and R. Courths, Surf. Sci. **370**, 293 (1997).

[4] O. S. Hernan, A. L. Vazquez de Parga, J. M. Gallego, and R. Miranda, Surf. Sci. **415**, 106 (1998).

[5] J. J. de Miguel, J. Camarero, J. de la Figuera, J. E. Prieto, and R. Miranda, in *Morphological Organization In Epitaxial Growth and Removal*, edited by Z. Zhang and M. G. Lagally (World Scientific, Singapore, 1998), p. 367.

[6] E. G. Moroni, G. Kresse, J. Hafner, and J. Furthmüller, Phys. Rev. B **56**, 15629 (1997).

[7] K. Kalki, D. D. Chambliss, K. E. Johnson, R. J. Wilson, and S.

Chiang, Phys. Rev. B **48**, 18344 (1993).
[8] S. Müller, P. Bayer, C. Reischl, K. Heinz, B. Feldmann, H. Zillgen, and M. Wuttig, Phys. Rev. Lett. **74**, 765 (1995); J. Giergiel, J. Shen, J. Woltersdorf, A. Kirilyuk, and J. Kirschner, Phys. Rev. B **52**, 8528 (1995).
[9] C. S. Fadley, *Basics Concepts of X-Ray Photoelectron Spectroscopy*, in *Electron Spectroscopy, Theory, Techniques and Applications*, edited by C. R. Brundle and A. D. Baker (Pergamon Press, New York, 1978), Vol. II, Chap. 1.
[10] F. Bruno, D. Cvetko, L. Floreano, R. Gotter, C. Mannori, L. Mattera, R. Moroni, S. Prandi, S. Terreni, A. Verdini, and M. Canepa, Appl. Surf. Sci. **162–163**, 340 (2000); F. Bruno, S. Terreni, L. Floreano, A. Cossaro, D. Cvetko, P. Luches, L. Mattera, A. Morgante, R. Moroni, M. Repetto, A. Verdini, and M. Canepa, Phys. Rev. B **66**, 045402 (2002).
[11] G. A. Rizzi, M. Petukhov, M. Sambi, and G. Granozzi, Surf. Sci. **522**, 1 (2003).
[12] L. Floreano *et al.*, Rev. Sci. Instrum. **70**, 3855 (1999); R. Gotter *et al.*, Nucl. Instrum. Methods Phys. Res. A **467-468**, 1468 (2001); An updated presentation of the beamline can be found at http: //www.tasc.infm.it/tasc/lds/aloisa/aloisa.html.
[13] E. Vlieg, J. Appl. Crystallogr. **33**, 401 (2000). The software is freely distributed at http://www.esrf.fr/computing/scientific/.
[14] F. Bruno, L. Floreano, A. Verdini, D. Cvetko, R. Gotter, A. Morgante, M. Canepa, and S. Terreni, J. Electron Spectrosc. Relat. Phenom. **127**, 85 (2002).
[15] M. Todorova, E. Lundgren, V. Blum, A. Mikkelsen, S. Gray, J. Gustafson, M. Borg, J. Rogal, K. Reuter, J. N. Andersen, and M. Scheffler, Surf. Sci. **541**, 101 (2003).
[16] F. U. Hillebrecht, J. C. Fuggle, P. A. Bennett, Z. Zolnierek, and C. Freiburg, Phys. Rev. B **27**, 2179 (1983).
[17] S. Tanuma, C. J. Powell, and D. R. Penn, Surf. Interface Anal. **21**, 165 (1993).
[18] M.-T. Lin, J. Shen, W. Kuch, H. Jenniches, M. Klaua, C. M. Schneider, and J. Kirschner, Surf. Sci. **410**, 298 (1998).
[19] S. Müller, B. Schulz, G. Kostka, M. Farle, K. Heinz, and K. Baberschke, Surf. Sci. **364**, 235 (1996).
[20] A. Biedermann, M. Schmid, and P. Varga, Phys. Rev. Lett. **86**, 464 (2001).
[21] D. Qian, X. F. Jin, J. Barthel, M. Klaua, and J. Kirschner, Phys. Rev. B **66**, 172406 (2002).
[22] R. Rochow, C. Carbone, Th. Dodt, F. P. Johnen, and E. Kisker, Phys. Rev. B **41**, 3426 (1990).
[23] B. Schirmer, B. Feldmann, and M. Wuttig, Phys. Rev. B **58**, 4984 (1998).